Available online at www.sciencedirect.com

ScienceDirect

Procedia CIRP 112 (2022) 322–327

www.elsevier.com/locate/procedia

14th CIRP Conference on Intelligent Computation in Manufacturing Engineering, Gulf of Naples, Italy

A preliminary account of electro-chemical machining of Ti-48Al-2Nb-2Cr produced by electron beam melting

Manuela Galati[a]*, Silvio Defanti[b], Nicolò Vincenzi[b], Giovanni Marchiandi[a], Andrea Gatto[b], Luca Iuliano[a]

[a]*Politecnico di Torino, Corso Duca degli Abruzzi 24, Torino 10129, Italy*

[b]*Università di Modena e Reggio Emilia, via P. Vivarelli 10, Modena 41125, Italy*

* Corresponding author. Tel.:0110904569. *E-mail address:* manuela.galati@polito.it

Abstract

Electron beam melting (EBM) made feasible γ-titanium aluminide (TiAl) alloys. However, the surface roughness resulting from EBM is poor, and the high mechanical properties make γ-TiAl difficult to be machined. Electro-Chemical Machining (ECM) is gaining interest as a finishing process to achieve low surface roughness. Based on the anodic dissolution mechanism, ECM realises a contactless material removal and results particularly suitable for difficult-to-cut materials. The paper investigates the use of ECM for the finishing of Ti-48Al-2Nb-2Cr, a γ-TiAl alloy made by EBM. The effects of current, voltage, feed rate and duty ratio have been accounted for under pulsed machining conditions.

Keywords: electro-chemical machining; titanium aluminide; electron beam melting; intermetallic; additive manufacturing; surface finish.

1. Introduction

Among the powder bed fusion (PBF) additive manufacturing process, electron beam melting (EBM) exploits the power of an electron beam for processing high-melting temperature alloys [1], as well as intermetallic materials as γ-TiAl [2]. In particular, these alloys, namely titanium aluminides, have gained extreme importance in the aerospace industry for the production of aircraft engine components, where the replacement of nickel-based superalloys opens impressive mass saving possibilities [3] and reduced time-to-fly and buy-to-fly ratios [4,5]. Besides the specific properties of strength and Young's modulus, compared to nickel-based superalloys, Titanium aluminides shows an excellent creep resistance at an application temperature ranging from 600°C to 800 °C [6]. Despite the great industrial interest, Titanium aluminide shows several drawbacks due to the manufacturing issues that make the production of components costly and challenging by conventional manufacturing processes [4]. On account of using a vacuum and hot working environment, EBM makes possible the production of crack-free components and homogenous mechanical properties compared to conventional casting [4]. However, the EBM process suffers from several downsides due to the low surface quality [7] and the low dimensional and geometrical accuracy [8]. Because of that, parts produced by the EBM process are still referred to as near-net-shape, and post-processing operations are required to achieve an acceptable level of finishing for aerospace applications [9]. In contrast to extensive research on TiAl alloy development, static and fatigue mechanical properties, oxidation and microstructure optimisation [6,10,11], the utmost

2212-8271
10.1016/j.procir.2022.09.103

functional advantages need to be supported by new research data on material machinability [3]. This aspect, both considering conventional or non-conventional processes, is still limited in the literature involving. The combination of high resistance at high temperature and the low ductility makes the Titanium aluminide difficult-to-cut materials [3], especially compared to other titanium alloys [12]. Broad research showed that the conventional machining of these alloys using contact cutting is significantly tricky because of the resulting poor tool life and the appearance of microcracks on the component surface [13]. To solve problems related to contact cutting, electro-chemical machining (ECM) may represent a viable alternative [14] since the material is removed thanks to a chemical reaction occurring between the anode workpiece and cathode tool in the presence of an electrolyte solution [5]. The main advantage of this technique is the potential of machining conductive materials regardless of their mechanical properties, such as hardness [15].

Additionally, high surface quality can be achieved with no tool wear and no thermal effects on the workpiece [15]. Conventional ECM utilises continuous DC voltage, usually between 6 V and 30 V. The electrolyte fed into the inter-electrode gap (IEG) is, typically, an aqueous solution of NaCl or NaNO3. Other than completing the electrolytic cell, the fluid is necessary to flush away the residues resulting from the ongoing chemical reaction. The achievable machining accuracy has been dramatically improved with the development of pulsed electro-chemical machining (PECM), thanks to a more uniform electric distribution across the gap [5,15].

Owing to these advantages, ECM is already applied in the aerospace industry as a finishing process for turbine blades [15] and gears [16]. Moreover, it is adopted for moulds and dies as well as in the production of medical devices. Particularly for aerospace applications with difficult-to-cut materials, a finishing option that does not involve any mechanical contact or thermal effect on the workpiece is highly desirable [17]. The benefits become even more pronounced if ECM is used to finish parts built by powder bed fusion (PBF). The complex and topology-optimised geometries manufactured by AM often include thin-walled structures that can easily be deformed by conventional tool machining [3,18]. A good example of the necessity of contactless finishing solutions is the manufacturing of lattice structures that represent one of the most promising developments in finishing PBF manufactured components [19]. It has been shown [20] that ECM of conventionally-produced TiAl can achieve high integrity surfaces. However, the choice of the electrolyte is critical to avoid surface passivation that occurs with chlorides.

The purpose of the present paper is to study the viability of ECM as a finished process for finishing parts produced by EBM and made by Ti-48Al-2Nb-2Cr, a γ-TiAl alloys, primarily used for the production of low-pressure turbine blades.

2. Materials and methods

2.1. Specimens production and ECM

The experiments consisted of the production of specimens, in the shape of discs, manufactured in Ti-48Al-2Nb-2Cr by an Arcam A2X, an EBM system, and subsequent finishing by ECM operation.

The discs were 5 mm thick, and the diameter was approximately 60 mm. A total of 10 specimens were produced in a single job by using Arcam standard Ti-48Al-2Nb-2Cr powder with a size ranging between 45 μm and 105 μm. The chemical composition is given in Table 1. The disks were manufactured with their axis (or the generatrix of the cylinder) perpendicular to the build direction, as illustrated in [4] in Figure 1A. The discs were attached to the start plate by volume support. The preheating temperature was set to 1050°C, and the layer thickness was equal to 90 μm. The specimens were fabricated by using only the hatching strategy with a line offset equal to 0.3 mm. The melting process parameter setting consisted of a reference current equal to 10mA (reference length 25 mm), a focus offset equal to 15mA, and a speed function of 40. Also, the scanning path was rotated by 90 degrees for every consecutive layer.

The finishing operations were carried out using an IMPULSE ECM 50 machine, supplied by pECM System LTD (Yorkshire, UK). The machine works with a maximum voltage of 24V, and a maximum current of 1000A. The system incorporates a numerical control that allows managing speed and position of the tool. The electrolyte was an aqueous NaCl solution, chosen due to low cost, safety and availability. The active end of the tool was a cylinder of CuCrZr alloy. The electrolyte was pumped in the IEG through a specifically designed PLA dispenser used to confine and direct the electrolyte flow so that the same electrolytic cell was adopted as in [4]. The density of the electrolyte was kept constant at 1.071 g/cm^3 through all the tests. For all the ECM tests, the initial IEG and the flow rate were fixed to 0.5 mm and 3.63 l/min, respectively. ECM was conducted in the dynamic mode under pulsed current by varying the following machining parameters: voltage (V), duty cycle (DC), feed rate (f) and machining depth (d). The latter being the final tool position if the zero of coordinates is set on the peaks of the as-built surface, where the tool contacts the surface to be machined. The ECM conditions studied during the experiments are listed in Table 2, together with sample nomenclature. The following code identified specimens: V(V)_DC(%)_f(mm/min) _d(mm). The fourth column in Table 2 shows the active machining time (AMT), calculated by multiplying the total machining time by the DC. The AMT is the effective time of current flow between the tool and the workpiece, when the time-off is subtracted.

Based on literature studies that showed a beneficial effect of high voltage on TiAl during ECM [11-12], the machine was operated at the highest voltage range available, to test high values of current density.

Table 1. Chemical compositions of the Ti-48Al-2Nb-2Cr, weight %.

Ti	Al	Nb	Cr
bal.	33.4	5.1	2.2

Table 2. Sample nomenclature and ECM process parameters

Sample	V (V)	DC (%)	AMT (s)	f (mm/min)	d (mm)
20_20_0.5_0	20	20	12	0.5	0
25_30_0.5_0	24	30	18	0.5	0
20_20_0.5_-0.5	20	20	24	0.5	-0.5
24_30_0.5_-0.5	24	30	36	0.5	-0.5
20_40_0.5_-0.5	20	40	48	0.5	-0.5
24_60_0.5_-0.5	24	60	54	0.5	-0.5
20_20_0.5_-1.0	20	20	36	0.5	-1.0
24_30_0.5_-1.0	24	30	48	0.5	-1.0
20_20_0.2_-0.5	20	20	60	0.2	-0.5
24_30_0.2_-0.5	24	30	90	0.2	-0.5

2.2. Characterisation

Each sample was inspected through the Nikon SMZ1270i Stereo Microscope (Nikon, Japan). The roughness of all the as-built samples and the corresponding EC machined surfaces were measured in accordance to ISO 25178-2 [14]. A Nikon LV 150 Confovis Microscope was used to assess the surface topography with the following configuration: 100x microscopic objective; scanned area of 2.424 mm x1.717 mm obtained by stitching 3x2 scan patches acquired using the double exposure method. A FALS filter [15] with a cut-off of 0.008 μm and 0.1-99.9% bilateral symmetric threshold filtering (for the removal of spikes) were applied to the maps after the form removal. The 3D average areal surface roughness (Sa) was then calculated on the maps. Surface homogeneity had been checked in advance to validate the operation. Moreover, reduced peak height (Spk) and reduced valley depth (Svk) were determined, as well as skewness (Ssk) and kurtosis (Sku). Owing to the heterogeneity of the as-built samples, the machining effectiveness was evaluated by a one-to-one comparison between the surface morphology before and after the ECM finishing of each sample.

The sample surface morphology of each specimen was observed under a scanning electron microscope (SEM; Quanta-200, Fei Company - Oxford Instruments, UK) in order to investigate the removal phenomena.

The experimental MRR was calculated by multiplying the removed volume by the material density, measured by Archimede's principle and equal to 4.071 g/cm^3. In its turn, the removed volume was determined from the depth and diameter of the imprint left by the electrode as determined via calibrated optical images and confocal microscopy.

Each sample was cut along a plane perpendicular to the ECMed surface and parallel to the growth direction in the EBM process. Polished sections were observed the Nikon SMZ1270i microscope, and measurements of peaks and valleys were taken on the calibrated images.

3. Results and discussion

The complete set of results is collected in Table 3, where the surface parameters are collected for each specimen in the as-built (AB) and machined (Mach.) condition. The morphology of the as-built specimens can be well appreciated through the polished section in Figure 1, where peaks as high as 200μm and very deep valleys (400-500μm) are spotted. The build direction during the EBM process (Z direction) is vertical in the image, as in all the polished sections that are shown for the machines specimens. On the lateral surfaces of the discs, cracks parallel to the layers are generated during the EBM process. The surface map acquired on the same as-built specimen through confocal microscopy is illustrated in Figure 2.

In terms of quantitative results, the ECM finishing provides a reduction of S_a of 50% and 49% for, respectively, sample 20_20_0.5_0 and 24_30_0.5_0. The sections of these in Figure 3A and 3B show that, even if the roughness decrease is consistent, the machining of peaks is almost complete while valleys are still noticeable. The same is seen in the surface maps in Figure 4A and 4B. The result is partially described by the values of S_{pk} and S_{vk}. After the processing, the peak reduction percentage is 64.4% for specimen 20_20_0.5_0 and 65.7% for specimen 24_30_0.5_0. On the other hand, the valley reduction is of only 30.1% for the specimen 20_20_0.5_0 and equal to 59.5% in the case of 24_30_0.5_0. It should be considered that confocal microscopy is likely to underestimate the depth of valleys, as in the case of narrow and deep cracks, the measurement can lose efficacy.

The sections of the samples 20_20_0.5_-0.5 and 24_30_0.5_-0.5 are shown in Figure 3C and 3B, and the surface maps in Figure 4C and 4D. For these specimens, the machining depth was extended 0.5 mm below the surface of the as-built workpiece. The results in Table 3 indicate an improved efficacy of the finishing process. In particular, for the sample machined with a voltage of 24V and a DC of 30%, the reduction of S_a is as remarkable as 78%. Both the section and the surface maps reveal a further progression of machining concerning the tests where the tool was stopped at d=0.

\

Table 3. Results for MRR and for the surface parameters for each sample in the as-built (AB) and machined (Mach.) conditions.

Sample	MRR	Sa (µm)		Ssk		Sku		Spk (µm)		Svk (µm)	
	mg/min	AB	Mach.	AB	Mach.	AB	Mach.	AB	Mach.	AB	Mach.
20_20_0.5_0	3.25	58.7	29.4	0.021	-0.245	2.650	3.060	66.0	23.5	59.1	41.3
24_30_0.5_0	3.86	57.1	29.3	-0.609	-0.445	3.600	3.100	53.4	18.3	109.0	44.1
20_20_0.5_-0.5	2.20	58.9	24.6	-0.456	-1.340	3.440	5.070	56.8	8.03	98.2	61.4
24_30_0.5_-0.5	1.93	80.1	17.8	-0.387	-0.173	2.660	3.180	52.8	19.7	112.0	26.4
20_40_0.5_-0.5	3.52	59.0	12.8	0.101	0.110	2.880	3.540	56.5	18.1	87.0	15.8
24_60_0.5_-0.5	5.95	65.7	5.1	0.744	-0.007	3.940	5.040	60.4	6.3	136.0	7.3
20_20_0.5_-1.0	1.41	65.8	13.5	-0.456	-1.340	3.440	5.070	56.8	8.0	98.2	61.4
24_30_0.5_-1.0	-	-	-	-	-	-	-	-	-	-	-
20_20_0.2_-0.5	1.48	64.1	9.9	0.214	-0.041	3.470	2.780	86.6	12.1	75.5	10.3
24_30_0.2_-0.5	1.85	62.9	6.0	-0.717	-0.149	3.840	3.240	44.7	6.2	113	7.9

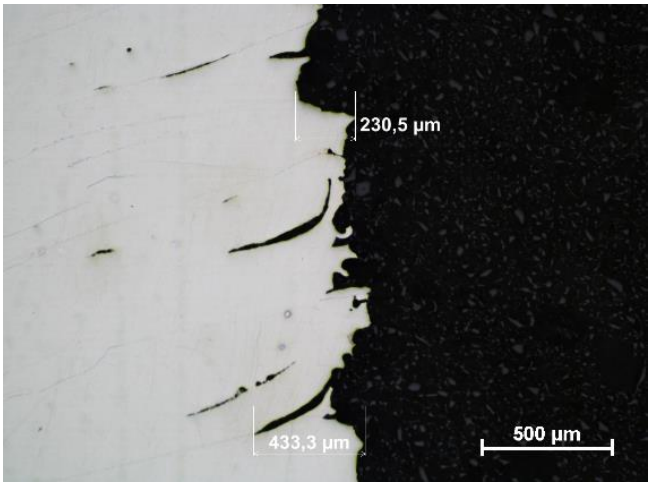

Fig. 1. Section of an as-built sample.

The samples 20_20_0.5_-1.0 and 24_30_0.5_-1.0 exploited an even increased machining depth. Owing to the extended tool path, the IEG for the latter test clogged, and for this reason, the test was aborted. However, the first test was conducted entirely and provided a S_a reduction similar to that achieved by stopping the tool at -0.5mm. The test 20_20_0.5_-1.0 was not included in Figures 3 and 4 due to the short-circuiting problems.

Increased DC was tested for the samples 20_40_0.5_-0.5 and 24_60_0.5_-0.5. These samples showed an impressive reduction of S_a that diminished by 78% and 92%, respectively. Moreover, as evinced by the value of S_{pk} and S_{vk} reported in

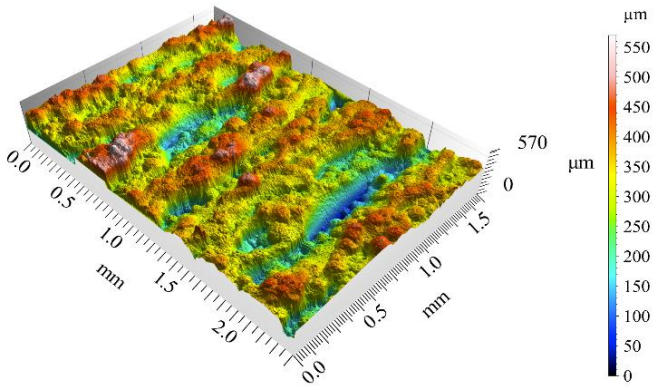

Fig. 2. 3D surface map of an AB sample.

Table 3, both the valleys and the peaks show a relevant reduction. The sections reported in Figure 3E and 3F and the maps in Figure 4E and 4F confirm that these ECM conditions provide a planar surface with no peaks or valleys.

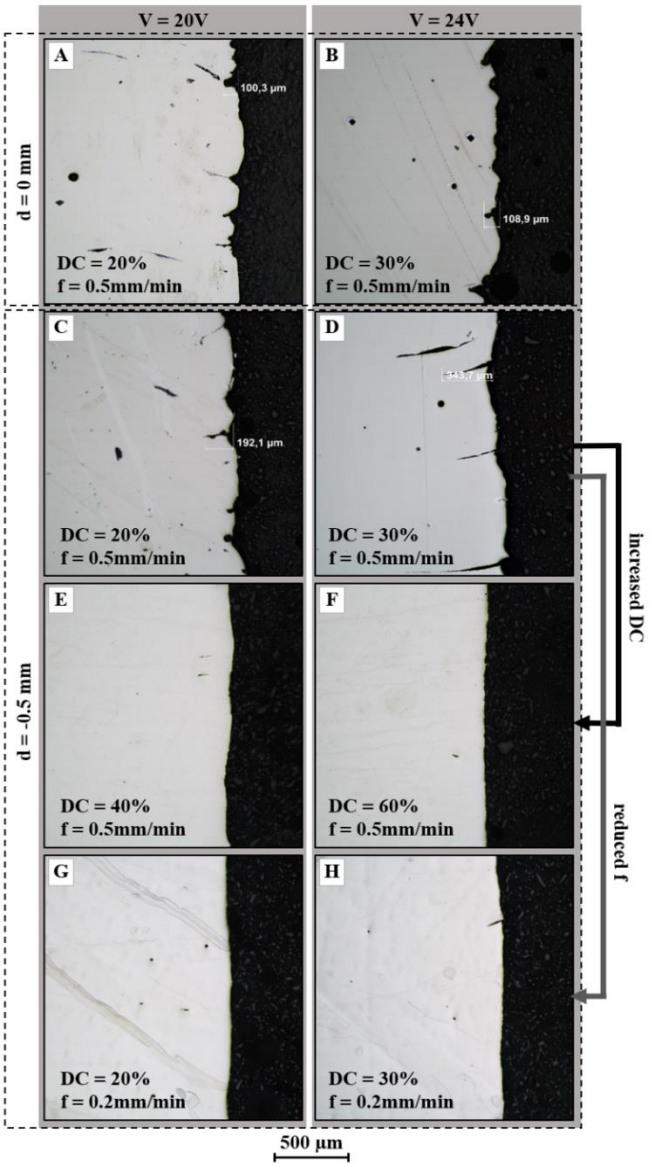

Fig. 3. Sections of ECMed samples: (A) 20_20_0.5_-0.5 (B) 24_30_0.5_-0.5, (C) 20_40_0.5_-0.5, (D) 24_60_0.5_-0.5, (E) 20_20_0.5_0, (F) 24_30_0.5_0, (G) 20_20_0.2_-0.5 and (H) 24_30_0.2_-0.5

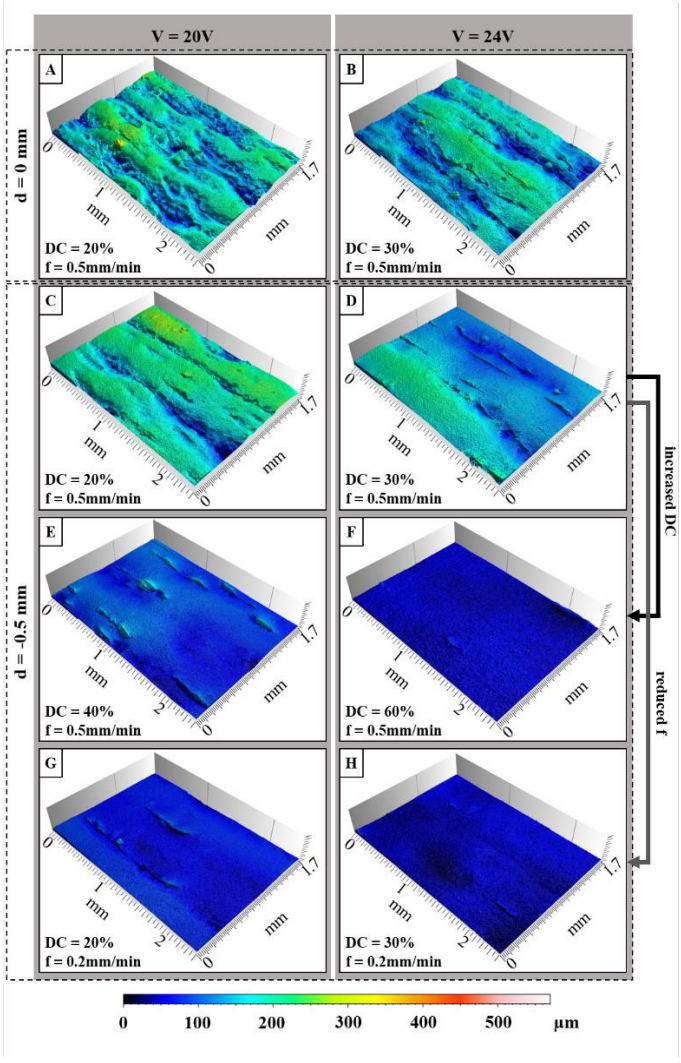

Fig. 4. 3D surface maps of the ECMed samples: (A) 20_20_0.5_-0.5 (B) 24_30_0.5_-0.5, (C) 20_40_0.5_-0.5, (D) 24_60_0.5_-0.5, (E) 20_20_0.5_0, (F) 24_30_0.5_0, (G) 20_20_0.2_-0.5 and (H) 24_30_0.2_-0.5

A lower feed rate was also tested for samples 20_20_0.2_-0.5 and 24_30_0.2_-0.5, to verify if the results with a higher DC were comparable to those with a lower speed, as both involve high values of AMT. The sections of these specimens are represented in Figure 3G and 3H. Similarly to what was attained with high DC, the lower feed rate accomplished a reduction of Sa of approximately 84% and 90%, and peaks and valleys underwent a similar diminishing.

Figure 5 illustrates the SEM image of the transition zone between the as-built surface and the finished counterpart. The image allows appreciating the progressive erosion phenomena. The removal of the material begins with the detachment of the satellite particles, proceeds by the dissolution of the peaks, followed by a flattening of the surface, as expected. However, due to the initial morphology of the as-built surface produced by EBM and to the memory effect [4], valleys are sometimes reproduced at a lower depth. The result is confirmed by the measurements taken on the calibrated images in Figure 3A-B-C-D, where the depth of valleys is in some cases maintained even for a machining depth that is nominally sufficient to erase completely the valleys measured on the as-built specimens. It can be reckoned that in all the tests with an AMT shorter than 40 s, the ECM process was stopped too early and was insufficient to flatten the initial morphology. Good results are initially obtained with the erosion of peaks, while valleys require further machining. Above that threshold of AMT, both an increase of the DC and a reduction of the feed rate allow the achievement of smooth surfaces. Further augmentation of the machining depth is not viable due to not optimal electrolyte flow through the IEG, insufficient removal of debris and short-circuiting. The result is that peaks are efficiently removed in the initial stages of the ECM process, but the erosion then stops prematurely.

\

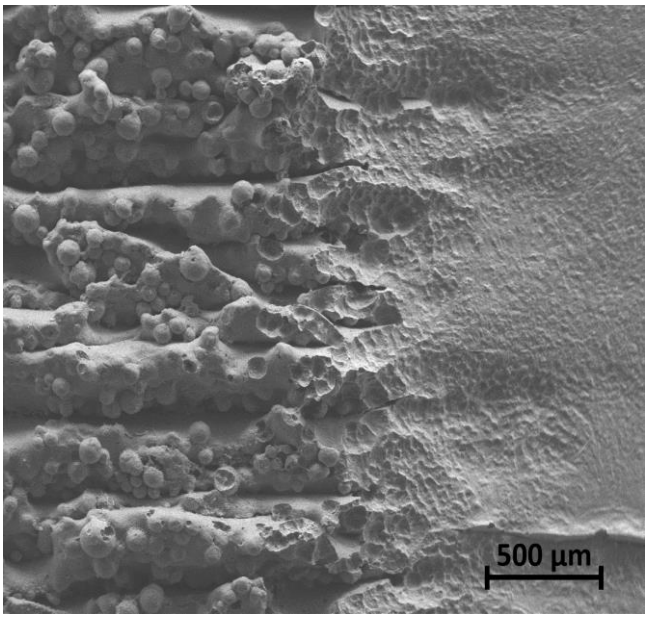

Fig. 5. SEM image of the AB-ECMed transition zone

The best results are obtained for the samples 24_60_0.5_-0.5 and 24_30_0.2_-0.5, with comparable values of areal surface roughness that is cut down to 5-6µm, and a highly effective flattening of peaks and removal of valleys. It is worth remarking that the two optimal machining conditions provide significantly different values of MRR. For equally smooth finished surfaces, the test 24_60_0.5_-0.5 benefits from more than 3 times higher productivity than for the test with reduced feed rate. In the considered conditions, a DC of 60% is not too high to hamper the flushing of the machining residues if the machining depth does not exceed -0.5mm.

If compared to literature data [21], similar values of MRR were measured. A comparison of the surface roughness values is instead impossible, as Klocke et al. [21] polished the specimens before the ECM process to remove the effect of the initial surface morphology.

4. Conclusions

Titanium aluminide was successfully machined by ECM, with a surface roughness reduction of approximately 90% in the best case. The optimal machining conditions were found to be a voltage of 24V, a machining depth of -0.5mm, and an active machining time between the 50s and 90s, achieved by acting on the duty cycle or the feed rate. With a DC of 60% and a feed rate of 0.05mm/min, the former also accomplishes very high productivity without any detrimental effect on the surface integrity.

References

[1] Körner C, Helmer H, Bauereiß A, Singer RF. Tailoring the grain structure of IN718 during selective electron beam melting. MATEC Web Conf., 2014. doi:10.1051/matecconf/20141408001.

[2] Körner C. Additive manufacturing of metallic components by selective electron beam melting—a review. Int Mater Rev 2016:1–17.

[3] Aspinwall DK, Dewes RC, Mantle AL. The machining of γ-TiAl intermetallic alloys. CIRP Ann - Manuf Technol 2005. doi:10.1016/S0007-8506(07)60059-6.

[4] Galati M, Iuliano L. A literature review of powder-based electron beam melting focusing on numerical simulations. Addit Manuf 2018;19:1–20. doi:10.1016/j.addma.2017.11.001.

[5] Rajurkar KP, Kozak J, Wei B, McGeough JA. Study of Pulse Electrochemical Machining Characteristics. CIRP Ann - Manuf Technol 1993. doi:10.1016/S0007-8506(07)62432-9.

[6] Murr LE, Gaytan SM, Ceylan A, Martinez E, Martinez JL, Hernandez DH, et al. Characterization of titanium aluminide alloy components fabricated by additive manufacturing using electron beam melting. Acta Mater 2010;58:1887–94. doi:10.1016/j.actamat.2009.11.032.

[7] Galati M, Minetola P, Rizza G. Surface Roughness Characterisation and Analysis of the Electron Beam Melting (EBM) Process. Materials (Basel) 2019;12:2211. doi:10.3390/ma12132211.

[8] Minetola P, Galati M, Calignano F, Iuliano L, Rizza G, Fontana L. Comparison of dimensional tolerance grades for metal AM processes. Procedia CIRP, 2020. doi:10.1016/j.procir.2020.05.069.

[9] Galati M, Rizza G, Defanti S, Denti L. Surface roughness prediction model for Electron Beam Melting (EBM) processing Ti6Al4V. Precis Eng 2021;69. doi:10.1016/j.precisioneng.2021.01.002.

[10] Biamino S, Penna A, Ackelid U, Sabbadini S, Tassa O, Fino P, et al. Electron beam melting of Ti–48Al–2Cr–2Nb alloy: Microstructure and mechanical properties investigation. Intermetallics 2011;19:776–81. doi:10.1016/J.INTERMET.2010.11.017.

[11] Baudana G, Biamino S, Ugues D, Lombardi M, Fino P, Pavese M, et al. Titanium aluminides for aerospace and automotive applications processed by Electron Beam Melting: Contribution of Politecnico di Torino. Met Powder Rep 2016;71:193–9. doi:10.1016/j.mprp.2016.02.058.

[12] Rahman M, Wong YS, Zareena AR. Machinability of titanium alloys. JSME Int Journal, Ser C Mech Syst Mach Elem Manuf 2003. doi:10.1299/jsmec.46.107.

[13] Uhlmann E, Frommeyer G, Herter S, Knippscheer S, Lischka JM. Studies on the Conventional Machining of TiAI-Based Alloys. Ti-2003 Sci. Technol. Vol. I Proc. 10th World Conf. Titan. Held CCH-Congress Cent. Hamburg, Ger. July 13-18, 2003, 2004.

[14] Sharman ARC, Aspinwall DK, Dewes RC, Clifton D, Bowen P. The effects of machined workpiece surface integrity on the fatigue life of γ-titanium aluminide. Int J Mach Tools Manuf 2001. doi:10.1016/S0890-6955(01)00034-7.

[15] Rajurkar KP, Sundaram MM, Malshe AP. Review of electrochemical and electrodischarge machining. Procedia CIRP, 2013. doi:10.1016/j.procir.2013.03.002.

[16] Huang L, Cao Y, Jia F, Lei Y. Research on spur face gear by electrochemical machining based on the complex surface mesh. Chaos, Solitons and Fractals 2020. doi:10.1016/j.chaos.2019.109443.

[17] Defanti S, Denti L, Vincenzi N, Gatto A. Preliminary assessment of electro-chemical machining for aluminum parts produced by laser-based powder bed fusion. Smart Sustain Manuf Syst 2020. doi:10.1520/SSMS20200039.

[18] Defanti S, Bassoli E. Repeatability of the fatigue performance of additively manufactured A357.0 under different thermal treatment conditions. Mater Sci Eng A 2021. doi:10.1016/j.msea.2020.140594.

[19] Sola A, Defanti S, Mantovani S, Merulla A, Denti L. Technological Feasibility of Lattice Materials by Laser-Based Powder Bed Fusion of A357.0. 3D Print Addit Manuf 2020. doi:10.1089/3dp.2019.0119.

[20] Clifton D, Mount AR, Jardine DJ, Roth R. Electrochemical machining of gamma titanium aluminide intermetallics. J Mater Process Technol 2001. doi:10.1016/S0924-0136(00)00739-1.

[21] Klocke F, Herrig T, Zeis M, Klink A. Comparison of the electrochemical machinability of electron beam melted and casted gamma titanium aluminide TNB-V5. Proc Inst Mech Eng Part B J Eng Manuf 2018. doi:10.1177/0954405416687147.